

**FABRICATION OF SCREEN PRINTED DOPED  
ZINC OXIDE THICK FILM ON METAL  
SUBSTRATE AS HEAT SINK FOR HIGH POWER  
LIGHT EMITTING DIODES**

**MAH JIAN WEN**

**UNIVERSITI SAINS MALAYSIA**

**2018**

**FABRICATION OF SCREEN PRINTED DOPED  
ZINC OXIDE THICK FILM ON METAL  
SUBSTRATE AS HEAT SINK FOR HIGH POWER  
LIGHT EMITTING DIODES**

by

**MAH JIAN WEN**

**Thesis submitted in fulfilment of the requirements  
For the degree of  
Master of Science**

**May 2018**

## ACKNOWLEDGEMENT

This Master thesis would not be complete successfully without the guidance and help from many scholars and industrial supervisor. I am truly grateful for the opportunity given in this research work. Through this research work, my research skills have greatly been improved due to the exposure of many cross-over discipline of fields.

First and foremost, I would like to express my deepest appreciation to my main supervisor, Assoc. Prof. Dr. Mutharasu Devarajan, co-researcher Dr. Shanmugan Subramani and co-supervisor Prof. Fauziah Sulaiman. I thank to my main supervisor for initiating this project with Collaborative Research in Engineering, Science and Technology (CREST) and choose me to be the research graduate under this project. His valuable guidance and motivation have steering me towards the correct direction. The freedom for me to grow in this project has made me a better researcher with sharp troubleshooting and decision making skills. Additionally, my sincere appreciation to Dr. Shanmugan and Prof. Fauziah for giving valuable inputs and advice within the research period. I am most grateful with the huge financial support provided by CREST under grant 304/PFIZIK/650696/C121 in completion of this research work. A million thanks to my Industrial Supervisor, Mr. Anba and ex-CEO of the Millennium Substrate Sdn. Bhd., Mr. Rema for your guidance and full support either in management or research skill within the duration of the project. Their vast experience in this field have widen my knowledge on thick film technology.

On the other hand, I would like to acknowledge the contribution and help from all the technicians and science officers in School of Physics, Institute of Nano-optoelectronics Research Lab (INOR) and Crystallography Lab for the technical support on the

characterization equipment. Despite being busy with their research routine, I would like to give my gracious thanks to my lab members who have faced the up and down in a hard way. My utmost gratitude to family's members for strong love, patience and financial support during the durations of my research. Finally, I would like to extend my thanks to the Engineers from Perkin Elmer Sdn Bhd for the guidance in TGA and FTIR characterization. Their support and guidance have answered all my doubts during my research period in the aforementioned characterization. There are many more people I would like to appreciate, while not listed here, for helping me during my difficulties.

## TABLE OF CONTENTS

Acknowledgement .....	ii
Table of Contents .....	iv
List of Tables .....	viii
List of Figures .....	ix
List of Plates .....	xv
List of Abbreviations .....	xvi
List of Symbols .....	xvii
Abstrak .....	xviii
Abstract .....	xx
<b>CHAPTER 1 - INTRODUCTION</b> .....	1
1.1 Overview .....	1
1.2 Introduction.....	1
1.3 Problem Statement .....	3
1.4 Objectives .....	4
1.5 Research Contribution .....	4
1.6 Thesis Outline .....	4
<b>CHAPTER 2 - LITERATURE REVIEW AND THEORITICAL</b>	
<b>BACKGROUND</b> .....	7
2.1 Overview .....	7
2.2 Thermal Challenges and Management in LED.....	7

2.3	Principle of 1D Heat Transfer in TIM .....	9
2.4	ZnO and its Doping.....	10
2.5	Co-precipitation Method of ZnO Powder .....	11
2.6	Co-precipitation of Metal doped ZnO Powder .....	12
	2.6.1 Al-doped ZnO.....	12
	2.6.2 Ag-doped ZnO.....	12
	2.6.3 Ca-doped ZnO .....	13
	2.6.4 Cu-doped ZnO .....	13
2.7	Film Deposition .....	13
	2.7.1 Thick Film Technology .....	14
2.8	Theory of X-Ray Diffraction .....	15
2.9	IR Spectroscopy .....	16
2.10	Thermal Transient Measurement .....	17
	2.10.1 Calibration and Measurement of LED Package .....	17
2.11	Reliability Testing.....	20
	2.11.1 Breakdown Voltage.....	20
	2.11.2 Effect of Moisture in Film.....	20
2.12	Summary .....	21
 <b>CHAPTER 3 - METHODOLOGY.....</b>		<b>23</b>
3.1	Overview.....	23
3.2	Synthesis of Pure and Metal-doped ZnO Powder.....	23
3.3	Preparation of Paste .....	26
3.4	Formation of Thick Film on Al Substrate.....	27

3.5	Sample Characterization and Testing .....	28
3.5.1	Characterization of Paste .....	28
3.5.1(a)	Thermogravimetric Analysis (TGA).....	28
3.5.1(b)	Rheological Testing .....	29
3.5.2	Characterization of Thick Film .....	29
3.5.2(a)	X-ray Diffraction Analysis .....	29
3.5.2(b)	Surface Morphology of Thick Film .....	30
3.5.2(c)	Surface Roughness of Thick Film.....	30
3.5.2(d)	FTIR.....	31
3.5.2(e)	Thermal Transient Testing .....	31
3.6	Reliability Testing.....	33
3.7	Summary .....	35
 <b>CHAPTER 4 – RESULT AND DISCUSSION.....</b>		<b>36</b>
4.1	Overview .....	36
4.2	Thermal Decomposition Analysis of Paste .....	36
4.3	Rheological Behavior of Paste .....	44
4.3.1	Influence of Different Combination of Filler and Binder on Paste .....	45
4.3.2	Influence of Different Metal-doped ZnO Filler on Paste .....	46
4.4	XRD Spectra of ZnO Thick Films .....	50
4.5	Surface Morphology and Topology of Thick Film.....	57
4.5.1	FESEM Analysis .....	57
4.5.2	AFM Analysis .....	63
4.6	FTIR of Thick Films .....	68

4.7	Thermal Characterization of Thick Films and Its Comparisons .....	71
4.7.1	Thermal Transient Analysis .....	71
4.7.1(a)	Influence of Applied Forward Current on Junction Temperature of different Thick Films .....	73
4.8	Reliability Testing.....	76
4.8.1	Breakdown Voltage Testing .....	76
4.8.2	Moisture Sensitive Testing (Level 1) .....	78
4.9	Summary .....	79
	<b>CHAPTER 5 –CONCLUSION AND RECOMMENDATIONS .....</b>	<b>80</b>
5.1	Conclusion .....	80
5.2	Recommendation for Future Research.....	81
	<b>REFERENCES.....</b>	<b>83</b>

**APPENDICES**

**LIST OF PUBLICATIONS**

## LIST OF TABLES

	<b>Page</b>	
Table 3.1	Composition of ZnO Paste for Thick Film Preparation	27
Table 3.2	Overview of Industrial Standards	34
Table 4.1	Total weight loss of $\alpha$ -Terpineol, ethyl cellulose and all pure and doped ZnO pastes	43
Table 4.2	Structure and other parameters of pure and metal-doped ZnO thick films at first three peaks	56
Table 4.3	Induced Strain and lattice parameters at (101) peak for all thick films	57
Table 4.4	Breakdown voltage of pure and doped thick films at 5.7kV	77
Table 4.5	Moisture sensitive testing of pure ZnO thick film	78

## LIST OF FIGURES

		<b>Page</b>
Figure 2.1	Thermal resistance model of LED package	9
Figure 2.2	(a) Thermal conduction for Fourier's Law and (b) actual TIM in electronics package	10
Figure 2.3	Schematic representation of wurtzite ZnO structure	10
Figure 2.4	Phenomenon of Bragg's Diffraction	15
Figure 2.5	Fundamental vibrational frequency of $\nu_1$ (symmetry stretching), $\nu_2$ (symmetry bending), and $\nu_3$ (antisymmetric stretching)	16
Figure 2.6	Relationship of Light Output with applied Forward Current and Voltage	17
Figure 2.7	(a) Heating and (b) Cooling schematic diagram of measuring LED in Thermal Transient Measurement	18
Figure 2.8	(a) Foster and (b) Cauer-type of representation of an RC network	19
Figure 2.9	Graphical presentation of thermal RC network in cumulative structural function graph	20
Figure 3.1	The preparation process of (a) pure and (b) metal-doped ZnO powders	24
Figure 3.2	Overall process for research flow chart	25
Figure 3.3	The preparation procedure for pure and metal-doped ZnO paste	27

Figure 3.4	Schematic representation of screen printing process. (a) placement of paste on screen (b) printing of paste via permeable perforations (c) paste is printed on substrate	28
Figure 3.5	Experimental setup for thermal transient testing	32
Figure 4.1	TGA result of $\alpha$ -Terpineol and ethyl cellulose	37
Figure 4.2	TGA results of different loading content of pure ZnO filler in paste	38
Figure 4.3	TGA Result of Al-doped ZnO paste with increasing doping concentrations	39
Figure 4.4	TGA Result of Cu-doped ZnO paste with increasing doping concentrations	40
Figure 4.5	TGA Result of Ca-doped ZnO paste with increasing doping concentrations	41
Figure 4.6	TGA Result of Ag-doped ZnO paste with increasing doping concentrations	42
Figure 4.7	Viscosity versus shear rate of $\alpha$ -Terpineol solution	45
Figure 4.8	Rheology result of (a) different filler loading of pastes (b) enlarge shear rate from 0 to 200s <sup>-1</sup>	46
Figure 4.9	Rheology result of Ag-doped ZnO paste with increasing doping concentrations	47
Figure 4.10	Rheology result of Al-doped ZnO paste with increasing doping concentrations	48
Figure 4.11	Rheology result of Ca-doped ZnO paste with increasing doping concentrations	49

Figure 4.12	Rheology result of Cu-doped ZnO paste with increasing doping concentrations	50
Figure 4.13	XRD pattern of Pure and Ca-ZnO thick film with different doping concentrations	52
Figure 4.14	XRD pattern of Cu-ZnO thick film with different doping concentrations	52
Figure 4.15	XRD pattern of Al-ZnO thick with different doping concentrations	54
Figure 4.16	XRD pattern of Ag-ZnO thic with different doping concentrations	54
Figure 4.17	Surface morphology of 45wt% pure ZnO thick film	58
Figure 4.18	Surface morphology of Al-ZnO thick film with (a) 3wt% (b) 5wt% (c) 7wt% and (d) 9wt%	59
Figure 4.19	Surface morphology of Ag-ZnO thick film with (a) 3wt% (b) 5wt% (c) 7wt% and (d) 9wt%	60
Figure 4.20	Surface morphology of Ca-ZnO thick film with (a) 3wt% (b) 5wt% (c) 7wt% and (d) 9wt%	62
Figure 4.21	Surface morphology of Cu-ZnO thick film with (a) 3wt% (b) 5wt% (c) 7wt% and (d) 9wt%	63
Figure 4.22	3D profile of 45wt% pure ZnO thick film	64
Figure 4.23	3D profile of all metal-doped ZnO thick films with various doping concentrations	64
Figure 4.24	Surface roughness of Ca-ZnO thick film with increasing doping concentration	66

Figure 4.25	Surface roughness of Al-ZnO thick film with increasing doping concentrations	66
Figure 4.26	Surface roughness of Ag-ZnO thick film with increasing doping concentrations	67
Figure 4.27	Surface roughness of Cu-ZnO thick film with increasing doping concentrations	67
Figure 4.28	FTIR spectra of Pure and Ca-ZnO thick film with increasing doping concentrations	69
Figure 4.29	FTIR spectra of Ag-ZnO thick film with increasing doping concentrations	69
Figure 4.30	FTIR spectra of Al-ZnO thick film with increasing doping concentrations	70
Figure 4.31	FTIR spectra of Cu-ZnO thick film with increasing doping concentrations	70
Figure 4.32	K-factor of LED used for Thermal Transient Characterization	71
Figure 4.33	Thermal transfer mechanism in term of thermal resistance	72
Figure 4.34	Junction temperature of control sample, pure and Ca-ZnO thick film with increasing applied forward current	73
Figure 4.35	Junction temperature of Cu-ZnO thick film with increasing applied forward current	74
Figure 4.36	Junction temperature of Al-ZnO thick film with increasing applied forward current	75
Figure 4.37	Junction temperature of Ag-ZnO thick film with increasing applied forward current	76

Figure A.1	Thermal resistance plot of control sample thick film with increasing applied forward currents.	94
Figure A.2	Thermal resistance plot of Ca-ZnO thick film with increasing concentrations at constant applied current of 250mA	94
Figure A.3	Thermal resistance plot of Ca-ZnO thick film with increasing concentrations at constant applied current of 500mA	95
Figure A.4	Thermal resistance plot of Ca-ZnO thick film with increasing concentrations at constant applied current of 750mA	95
Figure A.5	Thermal resistance plot of Ca-ZnO thick film with increasing concentrations at constant applied current of 1000mA	96
Figure A.6	Thermal resistance plot of Cu-ZnO thick film with increasing concentrations at constant applied current of 250mA	96
Figure A.7	Thermal resistance plot of Cu-ZnO thick film with increasing concentrations at constant applied current of 500mA	97
Figure A.8	Thermal resistance plot of Cu-ZnO thick film with increasing concentrations at constant applied current of 750mA	97
Figure A.9	Thermal resistance plot of Cu-ZnO thick film with increasing concentrations at constant applied current of 1000mA	98
Figure A.10	Thermal resistance plot of Al-ZnO thick film with increasing concentrations at constant applied current of 250mA	98
Figure A.11	Thermal resistance plot of Al-ZnO thick film with increasing concentrations at constant applied current of 500mA	99
Figure A.12	Thermal resistance plot of Al-ZnO thick film with increasing concentrations at constant applied current of 750mA	99
Figure A.13	Thermal resistance plot of Al-ZnO thick film with increasing	100

concentrations at constant applied current of 1000mA

Figure A.14	Thermal resistance plot of Ag-ZnO thick film with increasing concentrations at constant applied current of 250mA	100
Figure A.15	Thermal resistance plot of Ag-ZnO thick film with increasing concentrations at constant applied current of 500mA	101
Figure A.16	Thermal resistance plot of Ag-ZnO thick film with increasing concentrations at constant applied current of 750mA	101
Figure A.17	Thermal resistance plot of Ag-ZnO thick film with increasing concentrations at constant applied current of 1000mA	102

## LIST OF PLATES

	<b>Page</b>
Plate 3.1 Thermal Transient Tester (T3ster) equipment	33
Plate 3.2 Experimental Setup of Breakdown Voltage	34

## LIST OF ABBREVIATIONS

<b>1D</b>	one-dimensional
<b>AFM</b>	atomic-force microscopy
<b>ASTM</b>	American Society for Testing and Materials
<b>ATR</b>	attenuated total reflectance
<b>FESEM</b>	field Emission Scanning Electron Microscope
<b>FTIR</b>	fourier transform infrared spectroscopy
<b>FWHM</b>	full width at half maximum
<b>ICDD</b>	International Centre for Diffraction Data
<b>JEDEC</b>	Joint Electron Device Engineering Council
<b>LED</b>	light emitting diode
<b>RC</b>	resistor–capacitor
<b>rms</b>	root mean square
<b>SSL</b>	solid state lighting
<b>TIM</b>	thermal interface material
<b>wt</b>	weightage
<b>XRD</b>	X-ray diffraction
<b>Pa·s</b>	Pascal Second (Unit for Viscosity measurement)
<b>TGA</b>	thermogravimetric analysis
<b>T3ster</b>	thermal transient tester

## LIST OF SYMBOLS

$T_j$	junction temperature
$\Delta T_{JA}$	difference between junction temperature to ambient
$A$	cross-sectional area
$D$	crystallite size
$I_{drive}$	driving current
$I_f$	forward current
$I_s$	sensing current
$k$	thermal conductivity
$P_{el}$	applied electrical power
$Q$	heat flow
$R_a$	surface roughness
$R_{contact}$	thermal contact interface resistances
$R_{int}$	thermal resistance of TIM
$R_{th}$	thermal resistance of LED package
$t$	bone line thickness
$T_A$	ambient temperature
$V_f$	forward voltage
$\beta$	broadening of diffraction peak
$\delta T$	temperature gradient
$\delta x$	thickness
$\varepsilon$	internal strain
$\theta$	angle in radian
$\lambda$	Wavelength

**FABRIKASI PERCETAKAN SKRIN DOPED ZINC OXIDE FILEM TEBAL  
PADA SUBSTRAT LOGAM SEBAGAI SINK HABA UNTUK DIOD  
PEMANCAR CAHAYA KUASA TINGGI**

**ABSTRAK**

Satu jumlah haba yang besar terperangkap di dalam pakej Diod Pemancar Cahaya (LED) adalah akibat rintangan haba besar antara sumber haba dan sink haba. Rintangan haba besar ini telah mencipta sejumlah besar haba terkumpul di dalam pakej LED yang menyebabkan kecekapan bercahaya lemah, masa hidup LED lebih pendek, beralih panjang gelombang pelepasan dan isu-isu kebolehpercayaan. Biasanya, suhu simpang LED didapati kira-kira 120 °C pada aliran elektrik 250mA. Dalam projek ini, ZnO tulen dan empat logam ZnO didopkan filem tebal yang berbeza telah dicetak pada substrat Aluminium dengan teknik percetakan skrin menggunakan serbuk nano-kristal disintesis daripada kaedah pemendakan bersama. Serbuk logam didopkan dihasilkan daripada 3wt%, 5wt%, 7wt%, dan 9wt% daripada pendopan logam semasa proses pemendakan bersama. Serbuk yang disintesis dicampur dengan teliti dengan pelarut untuk membentuk pes tiksotrop dan skrin bercetak sebelum meneruskan kepada proses pembakaran. Pada peringkat awal, TGA menunjukkan penguraian terma pes ZnO tulen dan logam yang didopkan adalah di antara suhu pemanasan 119 °C dan 134 °C. 45wt% pes ZnO tulen telah dipilih kerana baki berat yang paling tinggi yang tertinggal selepas proses pemanasan. Kelakuan reologi pes ZnO tulen dan logam yang didopkan menunjukkan sifat tiksotrop yang mempunyai pengurangan kelikatan dengan peningkatan kadar ricih. Kelikatan awal 45wt% ZnO tulen pes telah direkodkan dalam

jarak dari 200 Pa·s ke 250 Pa·s, selaras dengan keperluan industri. Kesan penipisan ricih diperhatikan pada semua pes yang dihasilkan selepas kadar ricih  $200\text{s}^{-1}$ . Pembelauan sinar-X mengesahkan pembentukan ZnO dengan orientasi pilihan (101). Peralihan puncak corak XRD ke sudut Pembelauan yang rendah diperhatikan pada filem tebal didopkan kesan peningkatan kepekatan doping. Permukaan morfologi filem menunjukkan pembentukan lompong dan pengumpulan pengisi telah mengurangkan kecekapan pelepasan haba. Purata kekasaran permukaan filem tebal telah ditentukan dengan menggunakan mod ketukkan AFM. 9wt% Ca-ZnO filem tebal menunjukkan permukaan yang paling kasar pada semua filem tebal yang didopkan. FTIR menunjukkan kewujudan ikatan yang berbeza dalam filem tebal. Dari plot IR, sedikit peralihan pada kedudukan ZnO diperhatikan pada semua filem tebal logam didopkan. Prestasi haba fana pakej LED dengan filem tebal yang dicetak, disiasat dengan menggunakan aliran elektrik 250mA, 500mA, 750mA dan 1000mA merujuk kepada standard ASTM D5460. Penyambungan elektrik dari pakej LED ke T3ster dilakukan bagi perolehan data. Dari ujian haba fana, filem tebal ZnO tulen menunjukkan suhu simpang terendah LED pada semua arus hadapan. 3wt% Ca dan Cu-didopkan serta 7wt% Al dan Ag-didopkan ZnO filem tebal menunjukkan suhu simpang paling rendah di kalangan kepekatan doping yang lain. Pecahan ujian voltan filem tebal menunjukkan pelonjakan voltan rendah di kedua-dua filem ZnO tulen dan logam didopkan. Walau bagaimanapun, ujian sensitif kelembapan (tahap 1) menunjukkan bahawa tiada pengesanan wap air di dalam filem tebal yang dicetak selepas sampel filem tebal didedahkan di bawah  $85\text{ }^{\circ}\text{C} / 85\% \text{ rH}$  pada 168 jam mengikut standard industri.

**FABRICATION OF SCREEN PRINTED DOPED ZINC OXIDE THICK FILM  
ON METAL SUBSTRATE AS HEAT SINK FOR HIGH POWER LIGHT  
EMITTING DIODES**

**ABSTRACT**

A large amount of heat trapped inside Light Emitting Diode (LED) package is the consequence of large thermal resistance between the heat source and the heat sink. These large thermal resistances created a huge amount of heat accumulated inside the LED package resulting in poorer luminous efficiency, shorter life time, shifting of emission wavelength and reliability issues. Typically, the junction temperature of the LED was found to be approximately 120°C on 250mA of applied forward current. In this project, pure and four different metal-doped ZnO thick films were deposited on Aluminium substrate by screen printing technique using nano-crystalline powder synthesized from co-precipitation method. The metal-doped powders were produced from 3wt%, 5wt%, 7wt%, and 9wt% of metal dopant during the co-precipitation process. The synthesized powders were thoroughly mixed with solvent to form a thixotropic paste and screen-printed before proceeding to the curing and firing process. TGA showed that the initial stage of thermal decomposition process of pure and metal-doped ZnO pastes was between 119°C and 134°C of heating temperature. 45wt% of pure ZnO paste was chosen due to the highest remaining weight after the heating process. Rheological behavior of pure and metal-doped ZnO paste showed thixotropic properties by having decreasing viscosity with increasing shear rate. Initial viscosity of the 45wt% pure ZnO paste was listed in the range from 200 Pa·s to 250 Pa·s, in accordance with the

industrial requirement. Shear thinning effect was observed among all the produced pastes after applying shear rate of  $200\text{s}^{-1}$ . X-ray diffraction results confirmed the formation of ZnO with preferred orientation along (101) plane. Peak shifting to lower diffraction angle of XRD pattern was observed for doped thick films upon increment of doping concentration. Surface morphology of the films indicated that the formation of voids and aggregation of fillers had reduced the efficiency for heat dissipation. Average surface roughness of all thick films was determined by using AFM tapping mode. 9wt% Ca-ZnO thick film showed the roughest surface among all the doped thick films. FTIR plot showed the existence of different bonding in the thick film. From the IR plot, a slight shifting of ZnO position was observed for all the metal-doped thick films. The thermal transient performance of the LED package with the screen-printed thick films was investigated by applying 250mA, 500mA, 750mA and 1000mA of forward currents whereby the experiment setup was referring to ASTM D 5460 standard. Electrical connection was wired from the LED package to T3ster for data acquisition. From the thermal transient testing, pure ZnO thick film was shown to have the lowest junction temperature of the LED at all four different applied forward currents. 3wt% Ca and Cu-doped as well as 7wt% Al and Ag-doped ZnO thick films were found to have the lowest junction temperature among the other doping concentrations. Breakdown voltage testing of thick film showed that low voltage surging across both pure and metal doped ZnO films. However, moisture sensitive testing (level 1) reviewed that no detection of water vapor present inside the printed thick film after exposing the thick film samples under  $85^{\circ}\text{C}/85\%r\text{H}$  for 168 hours as per industrial standard.

## Chapter 1

### Introduction

#### 1.1 Overview

This chapter contains a brief introduction to the thermal challenges in light emitting diode (LED) and the current problems in this LED device. Additionally, the research objectives and the outline of the thesis as well as the contribution and output of the project are highlighted.

#### 1.2 Introduction

Maintaining good light quality and quantity have rose a considerable discussion among end users. Energy-efficient lighting option with same amount of light or less money is something that spurred household the most. In conjunction to emit energy-efficient light, a huge amount of heat energy will directly be created and cumulated in the luminaire. Hence, LED has stepped into the solid state lighting's (SSL) market in the past few years with outstanding advantages, for instance, long lifespan, lower power consumption, vibration insensitive, etc. which makes it an important light source for the next generation [1]. Currently, thermal performance of LED is actively studied and investigated both in academics and researcher in solid state industries in order to enhance its performance especially the heat dissipation of LEDs. Due to strong dependence of the light output of LEDs on its junction temperature, luminous efficacy and efficiency of the LED can greatly be improved by managing its thermal properties [2], [3]. However, due to miniaturization of the LED package, heat accumulated inside

the package has tremendously increased which necessitate better techniques of thermal management to be implemented inside the package.

In order to improve the thermal dissipation mechanism of the LED package, many industries have provided many kinds of heat dissipation solution for optoelectronics, like heat spreader, microchannel of heat sink and thermal interface material (TIM) [4]. In LED package, TIM is easily engineered and used to become an efficient thermal conducting material besides serving its main function as an electrical insulator. Currently, nano-structured materials had been explored as a means to improve the thermal and mechanical properties. Nano-composite materials had been incorporated in commercially available TIMs for improved thermal conductivity[5]. ZnO is a wide bandgap semiconductor material of the II-VI semiconductor group. It is insoluble in water however will dissolve in most acid or alkali medium. With its high melting point, ZnO will only decompose to Zn vapor at 1975°C, which highlights its strong temperature stability in nature. Since TIM has to be an electrical insulator, Zinc oxide (ZnO) has been used in this project, due to its wide application as dielectric ceramic and device capable of operating at high temperature [6]–[8].

In nature, ZnO tends to exist in hexagonal crystal structure, where Zn atom is tetrahedrally connected with four atoms in the lattice. The substitution of the Zn atom by dopant has been reported in many journals where new engineered material properties are created. The resistivity of the ZnO is assumed to be lowered down when doped with high thermal conductivity materials. Additionally, due to its chemical and temperature stability with additional feature like insulation towards electricity, it can be used as insulation layer for electronics devices [9]–[13].

### 1.3 Problem Statement

Due to the miniaturization of LED package, accumulation of heat inside the package has an impact on performance of the LED device, even in the case of small driving current. The resulting performance deterioration is expectedly worse for a high powered LED with a tremendous rise in junction ( $\Delta T_j$ ) and thermal resistance. Undesired effects include a drop in light output, brightness, lifespan and emergence of reliability problems at normal operating condition that can directly leads to failure of the LED package. Hence, dissipation of heat out from the package has to be carefully designed, in which one of the approaches is to fabricate a newly-engineered TIM with better performance. The development of a new TIM that can serve as both dielectric layer and thermally conductive path way is suggested. This proposed new TIM aims to conduct more heat than the market available TIM and hence reduce the junction temperature and thermal resistance of the LED package without compromising other parameters and following JEDEC 51 measurement standards. From the datasheet of the Osram Golden Dragon (LW W5SM) LED, it is reported that the junction temperature of  $135^\circ\text{C}$  has been tested at 350mA under  $25^\circ\text{C}$  of ambient temperature.

In thick film and electronics related industries, high firing temperature of dielectrics material ( $> 450^\circ\text{C}$ ) is practiced in the manufacturing line. The manufacturing cost has reduced the profit margin of the product for these industries. In the case of selection of substrate, usage of alumina and glass as substrate are popular among the thick film product. These substrates have to be annealed under  $600^\circ\text{C}$  to  $1100^\circ\text{C}$  in order to create good deposition despite of their expensive material cost. Instead of high material and manufacturing cost, the compatibility of the cover coat with dielectric layer with

conductor layer on top is always a concerning issue as it creates reliability problem in the future. In this project, low temperature fired thick film coating is deposited on Aluminium via screen printing technique has been proposed by using different pure and metal-doped ZnO thick films as cover coat (moisture resistance) besides performing as TIM for heat dissipation.

#### 1.4 Objectives

The objectives of this study are:

- To synthesis pure ZnO and metal doped ZnO powder using co-precipitation method.
- To fabricate pure ZnO and metal doped ZnO thick film on Aluminium (Al) substrate using screen printing technique with low temperature firing.
- To investigate the junction temperature of the LED package with the doped thick films deposited on Al substrate as heat sink.
- To study the breakdown voltage and moisture sensitivity of thick film deposited on Al substrate

#### 1.5 Research Contribution

At the end of this project, homogenous thixotropic pure and four different metal-doped ZnO pastes are produced. The pure and doped ZnO fillers are coated on Al substrate as thick films. Additionally, a low cost (RM 6.00 per piece) chemical synthesis technique of producing thick film is developed for the fabrication of dielectric layer. The prepared thick film coating can also be used a cover coating and TIM for electronics device.

#### 1.6 Thesis outline

This thesis was divided into six chapters, which were introduction, literature review, theoretical background, methodology, results and discussion and conclusion with recommendations.

i) Chapter 1: Introduction

This chapter addressed the general information regarding the challenges of LED device and the importance of thermal dissipation of LED. Objectives of this project were highlighted and linked to the performance of the LED with respect of junction temperature and thermal resistance of the LED.

ii) Chapter 2: Literature Review and Theoretical Background

In this chapter, the history of development of thermal interface material, starting from synthesis method of pure and doped ZnO powder till the formation of paste and thick films were explained. Additionally, a review of the previous works was extensively included. The fundamental on the pure and doped ZnO thick film with respect to their material properties, the basic of 1D heat transfer and its mechanism were explained in this chapter.

iii) Chapter 3: Methodology

Experimental details of producing pure and doped ZnO powders were explained in this chapter. The formation of paste and technical details regarding the screen printing process were also included in this chapter where some details were highly noticeable for better printing quality. After the printing process, characterization techniques were highlighted, so that the performance of the printed films was investigated in the next session.

iv) Chapter 4: Results and Discussion

In this chapter, the measured data from the characterization techniques were reported. The performance of the paste and thick film were explained based on its thermal decomposition profile, rheological, structural, surface, optical, and thermal characteristics.

v) Chapter 5: Conclusion and Recommendations

In the last chapter, all experimental works were summarized and the conclusion of this project was presented. Further recommendations and improvement were suggested to improve the printed thick film in the near future.

## Chapter 2

### Literature Review and Theoretical Background

#### 2.1 Overview

This chapter reports the approach in addressing the thermal challenges in LED packages and its solutions. Fundamental operating principle of one-dimensional (1D) heat transfer in TIM is highlighted as this creates better understanding of thermal conduction path in the LED package. On the other hand, synthesis and fabrication of ZnO powder and thick film are described through co-precipitation and screen printing techniques respectively. Apart from the review of literature in LED package and fabrication methods, explanation corresponds to the operating principle of thermal transient measurement is also elaborated in this chapter.

#### 2.2 Thermal Challenges and Management in LED

Due to the innovation driven by the advance in technology and concerns in energy-saving concept, LED is invented to replace the fluorescent light bulbs in general lighting application. Its outstanding advantages, for instance, long lifespan, lower power consumption, vibration insensitive, etc. which increases its application in various industries [14]. Based on the enhancements made since the first Gallium Nitride (GaN) LED was invented, lumen per watt of phosphor-based white LED has been pushed up to a level more than 320 lumen per watt from 50 lumen per watt [15]. With this excellent optical performance, maintenance of lifecycle and optical performance of the LED, reliability testing like thermal cycling in humid and temperature dependent environment have been carried out [16]–[19].

However, electronics devices and circuit dimensions have been greatly miniaturized, creating significant challenges like development of new materials, reliability testing, and investigation for package and system level that will lead to the understanding of thermal dissipation mechanism of the devices especially the LED package. In the thermal dissipation mechanism, thermal conduction provides significant cooling effect as compared to convection or radiation. Thus, thermal conduction between the heat source and the heat sink is the only way for the heat to be externally dissipated [20]. As most of the LED's chip cannot withstand more than 150°C of junction temperature, proper design of package had been considered [21]. Managing the thermal conduction path is an essential way to improve the performance of the device. Every part of the LED package, starting from the die of LED, die attach's material, heat spreader of housing, TIM and heat sink, has been extensively investigated for optimum heat removal [4]. From Fig. 2.1, a simplified thermal resistance network is shown for describing the thermal conduction mechanism of LED package [22]. Heat is generated at die and junction temperature,  $T_j$ , is measured corresponding to the thermal resistance at metal substrate,  $R_{\theta J-MS}$ . The heat slowly dissipates to the printed circuit board (PCB) with recorded thermal resistance,  $R_{\theta ms-PCB}$ . It is further dissipated to ambient via heat sink with the recorded thermal resistance,  $R_{\theta hs-A}$ . As illustrated in Fig. 2.2, TIM plays an important role in spreading the heat externally as it reduces the thermal contact resistance between the substrate and the heat sink [23]. The types of TIM in the market include grease, solder, polymer and phase change based materials [24]–[27].

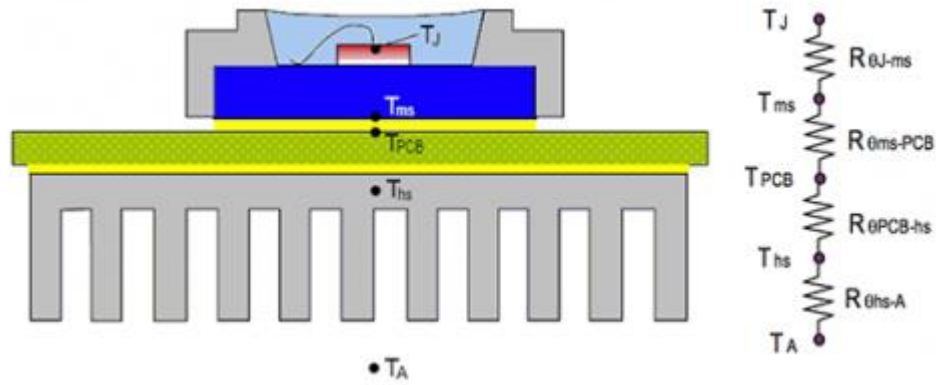


Figure 2.1 Thermal resistance model of LED package

### 2.3 Principle of 1D Heat Transfer in TIM

Thermal conduction takes place in all matters in which the heat flows from hotter to cooler medium. This phenomenon is explained by Fourier's Law of Heat Conduction as shown in Fig. 2.2 (a). Mathematically, it is presented in Eq. 2.1 where  $Q$  is the heat flow passing through cross-sectional area,  $A$ , with temperature gradient,  $\delta T$ , between hot,  $T_{hot}$ , and cold,  $T_{cold}$  temperature terminals,  $k$  is the thermal conductivity of the material and  $\delta x$  is the thickness along direction of  $x$ -axis.

$$Q = -kA \frac{\delta T}{\delta x} \quad (2.1)$$

In actual application shown in Fig. 2.2 (b), there are two thermal contact interface resistances,  $R_{contact}$ , between the heat source and the heat sink. In order to identify the thermal resistance of the TIM,  $R_{int}$ , Eq. 2.2 is used where  $t$  is the bone line thickness of TIM, and  $k_{TIM}$  is the thermal conductivity of TIM.

$$R_{int} = \frac{t}{k_{TIM}} + R_{contact 1} + R_{contact 2} \quad (2.2)$$

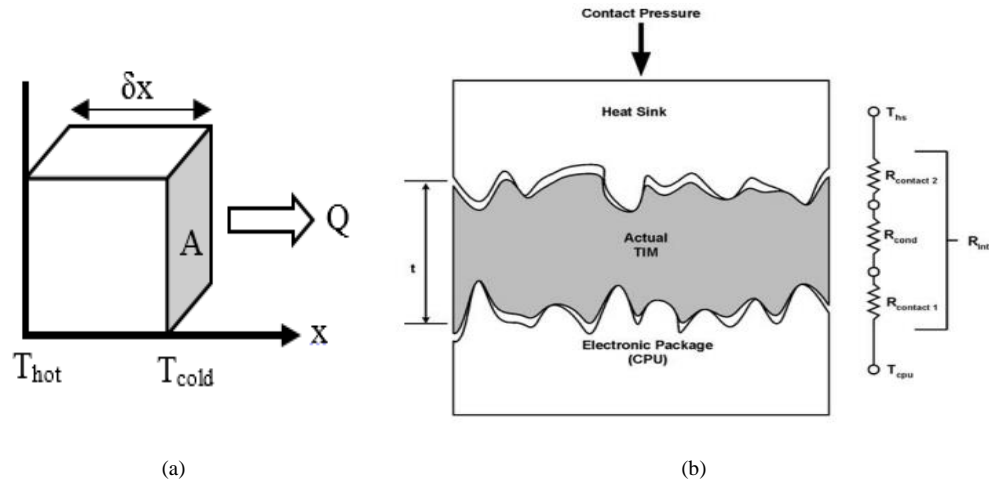


Figure 2.2: (a) Thermal conduction for Fourier's Law and (b) actual TIM in electronics package [28], [29]

## 2.4 ZnO and its Doping

ZnO has been studied since 1935, due to its remarkable properties and potential application in the electronics and optoelectronics industries. It is used as sensor, ceramics and luminescent material in many devices because of its good chemical stability and electrical insulation properties [30]–[32]. Additionally, ZnO exhibits several structures like nano-ribbon, nano-flower, nano-wire, and etc. [33]–[38]. At ambient temperature and pressure, ZnO crystallites in hexagonal wurtzite structure as shown in Fig. 2.3. This structure has one Zn ion to be surrounded by a tetrahedral of O ions.

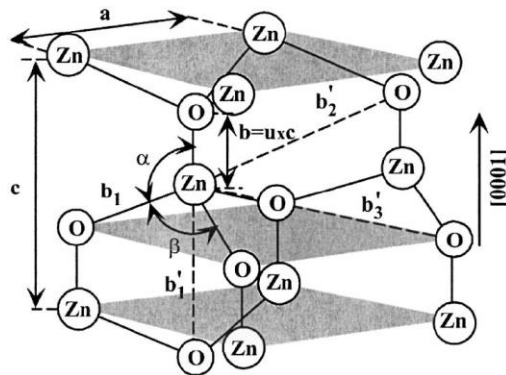


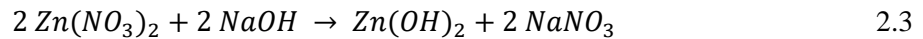
Figure 2.3 Schematic representation of wurtzite ZnO structure [39]

In the case of doping, the replacement of the Zn atom with high thermal conductivity element, like Al, Ag, Cu and etc., has been reported in many journals where new engineered material properties can be created [9]–[12], [40]. By changing the concentration of doping, conductivity, photosensitivity and luminescent properties can be enhanced [41]–[43]. Dopants can bond on the surface of ZnO nanostructure or integrate in its lattice structure [44]. Mannoj et al [45] has reported that the replacement of large radii Ca atoms in the ZnO lattice structure causes less deformation in the crystal. His research concludes that the introduction of Ca atom into the ZnO lattice structure has increased the conductivity of the sample. Similar assumption made by Ayadi et al, has proven the same increment of conductivity in their samples [46].

### 2.5 Co-precipitation Method of ZnO Powder

Co-precipitation method is a well-known method used to synthesis ZnO nano-structures powder as most ZnO powder are synthesized with high temperature method [47]. This method produces large quantity of ZnO powder with a low manufacturing cost [48], [49]. Numerous reports have suggested that nano-sized ZnO powder is synthesized [47], [50]–[54]. Raja et al used this method to synthesize of ZnO powder with an average of 37nm in size for optical application [47]. Kumar et al used Fe-doped ZnO powder synthesized via co-precipitation method to investigate the ferromagnetism properties of the powder. Their result concluded that their powder exhibited ferromagnetism at room temperature with DC magnetization measurement [53]. The chemical reaction of synthesis of ZnO, chemical equation is described in Eq. 2.3 [55]. With  $\text{Zn}(\text{NO}_3)_2 \cdot 6\text{H}_2\text{O}$  or any sulphate or

acetate of Zn as starting material, Zinc hydroxide,  $Zn(OH)_2$ , is produced which further react to form ZnO and water as described in Eq. 2.4 [56].



## 2.6 Co-precipitation of Metal doped ZnO Powder

### 2.6.1 Al-doped ZnO

Al-doped ZnO is used for transparent electrodes for electronics devices. Higher conductivity in films is reported after ZnO is doped with this doping material [57]–[59]. It is also used in low emissive windows as thermal insulator films. High optical bandgap and luminescence are observed with Al-doped nanoparticle, depending on concentration of doping and calcination temperature [60]–[65]. Chen et al studied the crystallization and physical properties of Al-doped ZnO nanoparticles. He concluded that the crystalline quality of ZnO deteriorated due to the stress generated from lattice disorder after heat treatment at temperature of 700°C with 5% of Al doping. The optical quality from PL measurement had decreased with increasing Al concentration at 800°C [64]. However, Tian et al reported that, the optical quality of Al-doped films had improved for films heated at 500°C [65].

### 2.6.2 Ag-doped ZnO

Ag-doped ZnO has been used in the photocatalytic and antibacterial research . In environment studies, Ag-doped ZnO is used as photocatalytic material to destroy the organic pollutants. Ruby et al used Ag-doped ZnO nanoparticles to mineralize organic compound into harmless simple mineral acids. Her studies also indicated that with ZnO

with 1mol% of Ag doping had more efficient photo-degradation property than pure ZnO and other samples with higher doping of Ag levels under ultraviolet light irradiation [66]–[68]. On the other hand, Karunakaran et al used Ag-ZnO nanoparticles to enhance antibacterial activities [69].

### 2.6.3 Ca-doped ZnO

Doping of Ca into ZnO has not gained much research interest among the research community. However, some researchers have found that doping of Ca can increase the conductivity of the sample. Mannoj et al reported that the insertion of large radii Ca atom into the ZnO lattice structures had resulted in less deformation in the crystal [45]. Similar assumptions made by Ayadi et al had proven the same increment of conductivity in their samples [70].

### 2.6.4 Cu-doped ZnO

Similar to Ag-doped ZnO, Copper is doped into ZnO for photocatalytic research [50]. Mittal et al reported that doping of Cu had improved the degradation process. Among the doping concentration, 3% of Cu showed the maximum photo-degradation of crystal violet dye. In addition to that, Muthukumaran and Gopalakrishnana studied the photoluminescence properties of Cu-doped ZnO. They stated that this nanomaterial can be used as tunable LED and other optoelectronics devices by controlling its properties. In their report, they suggested that the 6% Cu doping level showed better performance compared with other doping concentration [71].

## 2.7 Film Deposition

A variety of deposition methods to deposit ZnO thin film on various kinds of substrates has been reported. These methods include spray coating [72], [73], doctor-blade coating [74], [75], sputtering [76][77], sol-gel spin coating [78][79], chemical vapor deposition [80], [81], molecular beam epitaxy[82], [83], hydrothermal growth [84]–[86], and electrodeposition[87], [88], which have successfully produced thin layer within nanoscale in thickness. However, it is challenging to use the aforementioned methods to deposit ZnO film at a thickness of micron-scale. In order to deposit micron-scale film on a substrate, screen printing technique is used and discussed in the next subsection.

### 2.7.1 Thick Film Technology

Thick film technology had been used in the manufacturing of sensors in the signal processing industries since 90's [89]. As the miniaturization of electronics components is growing, many researches had been performed in this field [90]. The application of this technology in the deposition of ZnO on a substrate is demonstrated through the screen printing technique. This technique has reported to be one of the most cost effective and reliable technology for producing thick films on an industrial scale [91], [92]. This method has the ability to print on a variety of substrates available in the market, where the film thickness can precisely be monitored. In addition to that, complex design and pattern for printing can be easily achieved by this technology [93]–[97].

The quality of the printed film is mainly controlled by the nature of the paste, type of screen and the squeegee. Preparing a paste with rheological behavior suitable for screen printing is a major key factor. Both the material and mesh size need to be considered for uniform printing of the film[97]. Several journals have been published in regard to the

printing of ZnO paste. Lopez et al published that different behaviors of varistor was obtained by adding different percentages of loading content of ZnO with other additives in the paste. This group of authors had produced the paste with a ratio of 60wt% powder to 40wt% solvent. In the selection of organic vehicle, they used  $\alpha$ -Terpinol, ethyl cellulose and [2-(2-butoxi-etoxy-ethyl)] acetate upon mixing with the filler. The mixture showed thixotropic behavior of paste which was suitable for printing [98]. Krishanand Nampoori had used screen printed nanosized ZnO thick film for UV detectors and application in solar cells industry. They used ethyl cellulose as binder and  $\alpha$ -Terpinol as organic solvent, with the paste consisted of 30% powder and 70% solvent [98]. Liewhiran and Phanichphant had used similar material for paste making but they produced ZnO nanoparticles differently by using Flame Spray Pyrolysis method [99].

In the nutshell, the aforementioned benefits, like cost effectiveness in manufacturing, flexible selection of substrate for printing, suitable for complex design and pattern for printing and controllable thickness of film have become the reasons why thick film technology is chosen in this research work.

## 2.8 Theory of X-Ray Diffraction

Crystal is a regular array of atoms. When X-rays propagates to atom, scattering effect has occurred. The scattering wave of atoms produces array of spherical waves. These waves may cancel each other through destructive interference or may add constructively in which explained by Bragg's law as shown in Fig. 2.4. X-ray diffraction is resulted from X-ray impinging on array of scattered atoms.

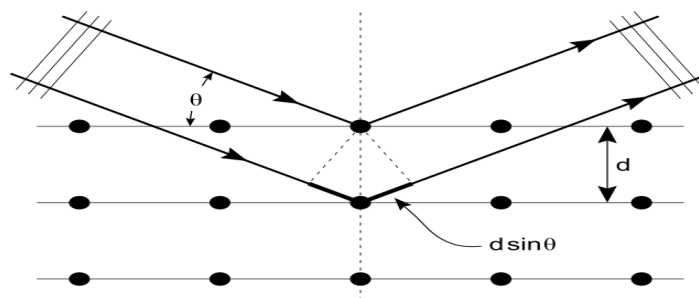


Figure 2.4 Phenomenon of Bragg's Diffraction

## 2.9 IR Spectroscopy

Infrared (IR) spectroscopy involves the interaction of infrared radiation with matter. It is used to identify the type of functional groups present in the tested sample. In wave mechanics, vibrational molecule can be considered as in a first approximation in which harmonically vibrating at  $(3N-6)$  simple harmonic motion, whereby  $N$  refers to number of atomic molecule. For simplicity of explanation,  $H_2O$  is used to explain the fundamental vibrational of atom. Each atom of water molecule needs three coordination for specifying its position in a 3D space. The  $3N-6$  of water molecule specifies the existence of three vibrational mode instead of three translation and rotation motion. These three-fundamental vibrations of water molecule are illustrated in Fig. 2.5.

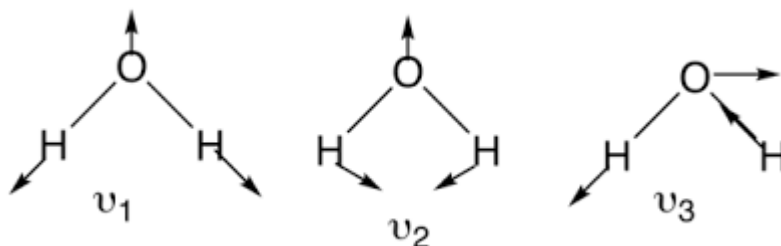


Figure 2.5 Fundamental vibrational frequency of  $\nu_1$  (symmetry stretching),  $\nu_2$  (symmetry bending), and  $\nu_3$  (antisymmetric stretching)

In this research work, Fourier Transforms Infrared (FTIR) spectroscopy is used to obtain the infrared spectrum of the adsorption or emission of matter. The beam that transmitted out from FTIR spectroscopy equipment contains full IR spectrum to be measured. It is shined into Michelson interferometer and beamed out with different spectrum that can be further processed into light absorption graph for each wavelength.

## 2.10 Thermal Transient Measurement

Junction temperature has become the major factor in determining the performance of any semiconductor device. In solid state lighting, like LEDs, junction temperature has become an indicator of thermal performance where the light output is strictly dependent on it. The relationship of light output and junction temperature corresponding to applied forward current and voltage is outlined in Fig. 2.6 [23]. Essential data, for instance, thermal behavior of components at package, board and system level, are obtained through thermal measurement. This information can help engineers to evaluate the thermal properties of TIM and other materials in the devices [100].

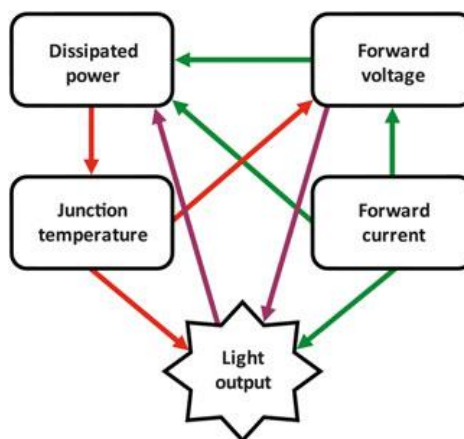


Figure 2.6 Relationship of Light Output with applied Forward Current and Voltage [101]

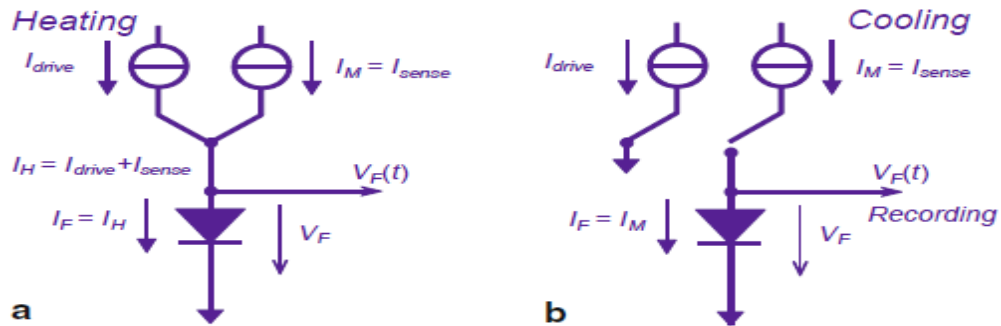
### 2.10.1 Calibration and Measurement of LED Package

Calibration of the LED is performed before the thermal transient measurement. The LED is placed in a thermostat and powered with 1mA of sensing current,  $I_s$ . The range of temperature used in calibration is from room temperature to 80°C. From theory, calibration of LED is named as K-factor, K. It is stated as the ratio of forward voltage,  $\Delta V_f$ , passing the device under test to temperature difference,  $\Delta T$  at constant sensing current, as described by Eq. 2.5.

$$K = \frac{\Delta V_f}{\Delta T} \quad (2.5)$$

While performing the measurement of LED package, the LED is placed under a still-air environment with constant ambient temperature,  $T_A$ . Initially, the LED is heated up by applying constant forward current,  $I_f$ , for a fixed duration of time. The applied forward current consists of driving current,  $I_{drive}$ , and sensing current,  $I_s$  as explained in Eq. 2.6.

$$I_f = I_{drive} + I_s \quad (2.6)$$



The LED is immediately measured by using sensing current after switching off the heating power. The measurement of LED is preferred to be done during the cooling state as only a small amount of  $V_f$  is used for sensing purpose. Additionally,  $V_f$  across the diode changes significantly during heating stage due to the switching between bigger

heating current and smaller sensing current. The LED measurement with the switching between heating and cooling stage is presented in Fig. 2.7.

Figure 2.7 (a) Heating and (b) Cooling schematic diagram of measuring LED in Thermal Transient Measurement [100]

Interestingly, the operation of thermal transient measurement is based on the representation of RC network, named as Foster-Cauer transformation. This network describes the heat conduction path and thermal impedance of the entire heat flow path which is displayed in Fig. 2.8 [102], [103]. By interpreting the RC network measured from the LED, thermal resistance,  $R_{th}$ , and thermal capacitance,  $C_{th}$ , of the physical material inside the LED package are determined. Each thermal resistance and capacitance are corresponded to one type of material. Hence, the obtained thermal resistance and capacitance are used to create a cumulative structural function graph which is shown in Fig. 2.9. Interpretation of the cumulative structural function graph results in the thermal resistance value of the LED package,  $R_{th}$ . In Fig. 2.9, the heat conduction path of the package ends at ambient, where infinite heat sinking capacity and therefore the thermal capacitance tends to approach infinity. Each gradient along the x-axis in the cumulative structural function graph represents a distinctive material in the graph. With the knowledge of thermal resistance of LED package, junction temperature of the die of the LED can be calculated by using Eq. 2.7, where  $\Delta T_{JA}$  is the difference between junction temperature to ambient, and  $P_{el}$  is the applied electrical power to the LED.

$$R_{th} = \frac{\Delta T_{JA}}{P_{el}} = \frac{T_J - T_A}{I_F V} \quad (2.7)$$

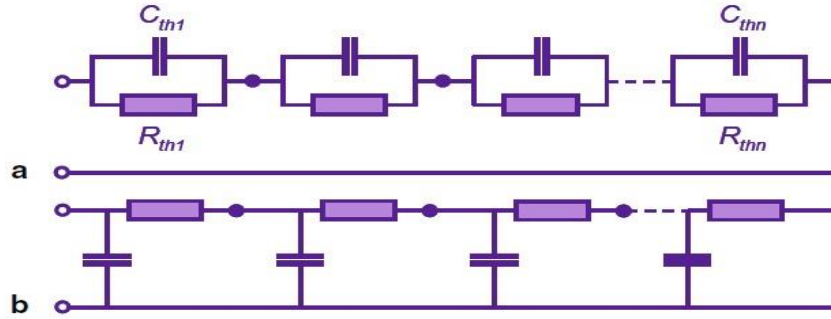


Figure 2.8 (a) Foster and (b) Cauer-type of representation of an RC network [104]

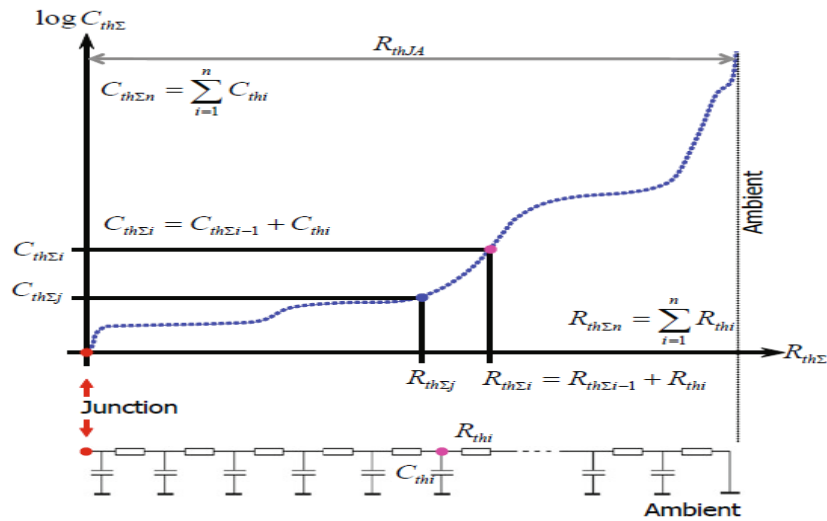


Figure 2.9 Graphical presentation of thermal RC network in cumulative structural function graph [102]

## 2.11 Reliability Testing

### 2.11.1 Breakdown Voltage

Breakdown voltage is the measurement of minimum voltage of an insulator that causes an insulator to become electrically conductive. In an actual application like dc power cable, the breakdown mechanism of the cable has to determine so that there is no leakage of current. To explain further on the breakdown mechanism of the thick film, Avalanche effect is used. Materials can conduct electricity if sufficient mobile charge carriers are present. When voltage gradient is applied between sample material and grounding, electron will move towards the positive terminal while hole will move to

negative terminal. If the strong electric field is applied, the applied current will create Avalanche phenomenon by conducting the material electrically. This process will then lead to the breakdown of the material and continue to conduct even if the voltage drops beyond the breakdown voltage. Yoshinobu et al had reported to measure the breakdown voltage of low-density polyethylene (LDPE) containing nano-filler of magnesium oxide [105]. In his report, the sample was subjected to a high DC voltage of 500V per second. Upon detection of leakage current, the breakdown voltage of the sample was recorded.

#### 2.11.2 Effect of Moisture in Film

Degradation is an alarming concern for any electronics devices as it will degrade at higher operating ambient temperature with the presence of moisture and oxygen. The water content inside the insulating material will increase the electric conductivity and lead to leakage of current which can create reliability issue [106]. For film substrate, existence of moisture inside the film can change the properties of the TIM in which weaken the mechanical strength of the TIM. This phenomenon will induce the cracking of TIM and affect the other component in the package to be degraded [107]. Hence, the presence of moisture in the produced sample is measured in this research work.

#### 2.12 Summary

Due to the known challenges experienced by the failure testing, thermal management of LED package has been extensively studied in order to improve its performance and lifespan. Thermal dissipation mechanism with respect to the cross sectional of the LED package has provided significant information for proper design and selection of material used in LED package. The fabrication of TIM has affected the heat dissipation in either 1D heat transfer or 2D spreading transfer. 1 D heat transfer in TIM is not adequate to

represent the thermal resistance of the package as it does not account the spreading effect in between the heat sources. Linear superposition method has to be employed in order to incorporate the transfer resistance between heat source on place which can fully understand the thermal resistance of the package. The overall performance of pure and doped ZnO thick films are related to interconnection of preparation of powder and paste, selection of dopants during powder making process, screen printing of film on Al substrate and film characterization, especially thermal transient measurement.

## Chapter 3

### Methodology

#### 3.1 Overview

The main focus of this research work is to obtain the experimental results on the behavior of the printed thick film dielectrics which act as heat spreader. In this chapter, experimental procedure from the formation of pure and metal-doped ZnO powders and pastes are described by co-precipitation method. This method was used by Kolthoff since 1932 [108]. It was popular due to its function to get precipitates or called as impurities in the fastest way in making powder in analytical chemistry. The produced precipitates were polycrystalline in nature. Its simplicity to replace one of the atom in the lattice structure during the crystal growth had contributed to its advantage in which reduced a lot of experimental duration in doping process when compared to CVD, MOCVD or MBE regardless of their crystalline quality. Screen printing technique for the deposition of the produced pastes and characterization techniques were explained. Overall process flowchart for this research project was shown in Fig. 3.2.

#### 3.2 Synthesis of Pure and Metal-doped ZnO Powder

The powder was formed using co-precipitation method, where all materials used in this research work were supplied by Sigma Aldrich with no further purification. Zinc (II) nitride,  $\text{Zn}(\text{NO}_3)_2 \cdot 6\text{H}_2\text{O}$ , and Sodium Hydroxide, NaOH, were separately dissolved in de-ionized water. NaOH solution was slowly added in drop wise manner into the pure Zinc (II) Nitride solution. The prepared solution was stirred at 80°C for 1 hour to form white precipitation. The white precipitate was further filtered and washed with ethanol

and distilled water. Filtered white powder was immediately dried at 120°C for 4 hours in oven so that the produced powder was free from the formation of zinc hydroxide.

For the preparation of the metal doped ZnO powder, metal dopants, such as aluminium (Al), silver (Ag), copper (Cu), and calcium (Ca), are selected due to their high thermal conductivity in nature. The reactants chosen were aluminium chloride hexahydrate,  $\text{AlCl}_3 \cdot 6\text{H}_2\text{O}$ , silver nitrate,  $\text{AgNO}_3$ , calcium nitrate tetrahydrate,  $\text{Ca}(\text{NO}_3)_2 \cdot 4\text{H}_2\text{O}$ , and copper (II) acetate monohydrate,  $\text{Cu}(\text{CO}_2\text{CH}_3)_2 \cdot \text{H}_2\text{O}$  for the different doping materials of Al, Ag, Ca, and Cu respectively. The reactants corresponding to different metal dopants were mixed with  $\text{Zn}(\text{NO}_3)_2 \cdot 6\text{H}_2\text{O}$  in de-ionized water before reacting with NaOH solution during the co-precipitation method. Four different doping concentrations of 3wt%, 5wt%, 7wt% and 9wt% were selected for each dopant. The resulting solution then followed the same experimental procedure of filtration and drying for the forming the precipitate powder. The preparation process is shown in Fig. 3.1.

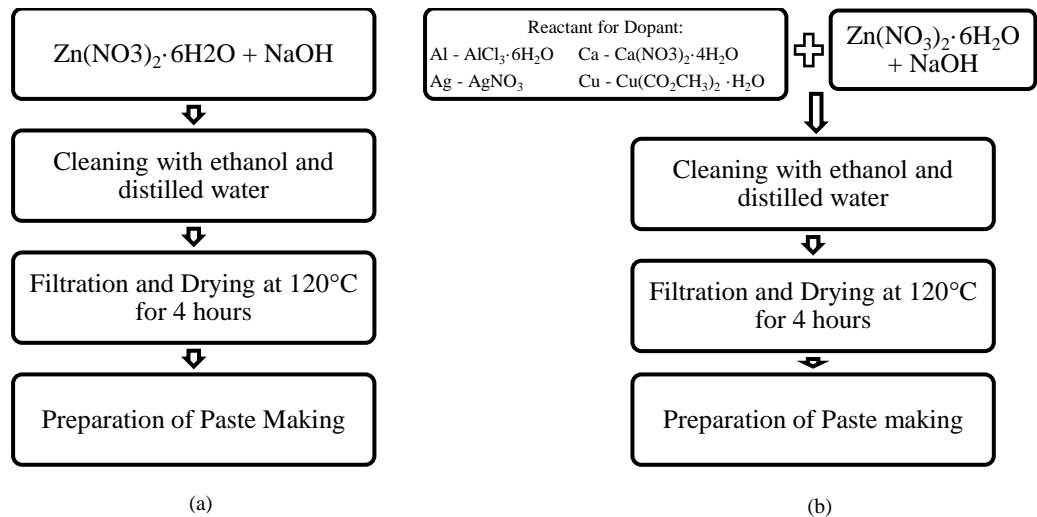


Figure 3.1 The preparation process of (a) pure and (b) metal-doped ZnO powders.